

Robust Latent Matters: Boosting Image Generation with Sampling Error Synthesis

Kai Qiu^{1*} Xiang Li^{1*†} Jason Kuen² Hao Chen¹ Xiaohao Xu³
Jiuxiang Gu² Yinyi Luo¹ Bhiksha Raj^{1,4} Zhe Lin² Marios Savvides¹
Carnegie Mellon University¹, Adobe Research², UMich³, MBZUAI⁴

Abstract

Recent image generation schemes typically capture image distribution in a pre-constructed latent space relying on a frozen image tokenizer. Though the performance of tokenizer plays an essential role to the successful generation, its current evaluation metrics (e.g. rFID) fail to precisely assess the tokenizer and correlate its performance to the generation quality (e.g. gFID). In this paper, we comprehensively analyze the reason for the discrepancy of reconstruction and generation qualities in a discrete latent space, and, from which, we propose a novel plug-and-play tokenizer training scheme to facilitate latent space construction. Specifically, a latent perturbation approach is proposed to simulate sampling noises, i.e., the unexpected tokens sampled, from the generative process. With the latent perturbation, we further propose (1) a novel tokenizer evaluation metric, i.e., pFID, which successfully correlates the tokenizer performance to generation quality and (2) a plug-and-play tokenizer training scheme, which significantly enhances the robustness of tokenizer thus boosting the generation quality and convergence speed. Extensive benchmarking are conducted with 11 advanced discrete image tokenizers with 2 autoregressive generation models to validate our approach. The tokenizer trained with our proposed latent perturbation achieve a notable 1.60 gFID with classifier-free guidance (CFG) and 3.45 gFID without CFG with a ~400M generator. Code: <https://github.com/lxa9867/ImageFolder>.

1. Introduction

In recent years, autoregressive (AR) generative modeling [69] has gained widespread adoption across various domains, such as text generation [1], speech synthesis [8, 50], and image generation [15]. It has emerged as a leading paradigm for the creation of high-quality content [7]. The

*Equal contribution.

†Now at Google DeepMind.

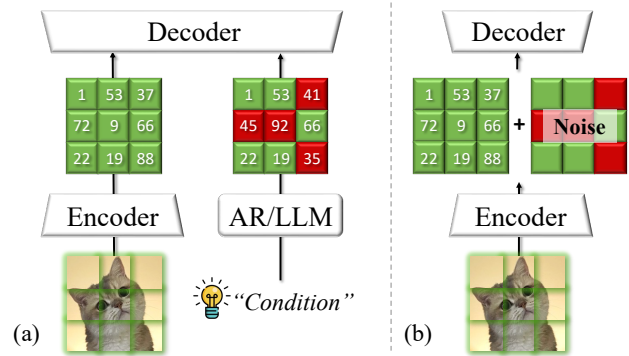


Figure 1. (a) Traditional image generation scheme: a discrete image tokenizer is first trained with reconstruction target where visual decoder is fed with clean image tokens. After that, an AR/LLM is trained with clean tokens under teacher forcing. However, during subsequent AR prediction (inference), unexpected tokens can be sampled from the learned distribution and challenge the robustness of frozen visual decoder. (b) RobustTok leverages latent perturbation to enhance the robustness of tokenizer, thus boosting the image generation quality.

success of AR models can be largely attributed to a two-stage training process: input tokenization with a tokenizer [23, 28, 40–42, 63, 76, 81–83, 88, 89, 91] and subsequent AR modeling and generation on the discrete latent space of the tokenizer [2, 76, 84].

Unlike diffusion models [11, 60], which operate directly on continuous representations [44, 49, 56, 67] through a denoising process, AR models typically rely on discrete tokens quantized by the tokenizer. These discrete tokens facilitate the modeling of latent distribution and subsequent sampling through next-token predictions [68, 69]. Despite the efficiency in generation [64], AR models suffer significantly from error accumulation [17, 55], mainly due to the discrepancies between the training and inference conditions. Specifically, AR models are usually trained under teacher forcing [62], where each prediction is based on the preceding ground truth tokens. In contrast, during inference, predictions rely solely on previously generated tokens, making even minor early errors to propagate and ac-

accumulate, and resulting in sampling error, *i.e.*, unexpected tokens being sampled during the AR inference process.

This issue is further amplified by the typically distinct and misaligned objectives of tokenizer training and AR inference. Tokenizer training prioritizes reconstruction fidelity where the visual decoder takes *clean* image tokens for accurate image reconstruction. Instead, to decoder tokens from a well-trained AR model, the sampling error occurs in the predicted tokens which makes the decoder takes *noisy* and potentially unseen latent patterns (Fig. 1 (a)). It necessitates the latent space to demonstrate sufficient robustness to handle the potential sampling errors. This divergence in objectives also results in a poor correlation between the reconstruction quality metrics [75], such as rFID, and the generative performance metrics [20], such as gFID, an issue repeatedly observed in recent literature [76, 84]. More recent research also demonstrated that the semantic information contained in latent tokens [35] and the structure of the latent space [6] can significantly influence the performance of generative models more than reconstruction metrics alone. Despite these insights, there still lacks a tokenization metric that explicitly captures the quality of the subsequent generation and guides improvements in AR generative modeling.

In this paper, we provide the first comprehensive exploration of how discrete latent space quality affects autoregressive generative modeling. Through rigorous analysis, we identify that AR error propagation primarily arises from insufficient robustness in discrete latent spaces. Motivated by this insight, we propose perturbed FID (pFID), a novel tokenizer evaluation metric designed specifically to measure the discrete latent space robustness under synthesized sampling error. As shown in Fig. 4, pFID effectively correlates and thus predicts downstream generative modeling performance, saving substantial cost to evaluate tokenizers by avoiding generator training.

Building upon these insights, we further introduce a latent perturbation method for tokenizer training (Fig. 1 (b)) to directly enhance the robustness of latent tokens, thereby significantly mitigating the downstream AR error accumulation and thus improving generation quality. Specifically, we propose a novel plug-and-play tokenizer training strategy that systematically integrates latent perturbations with an annealing schedule, gradually reducing perturbation intensity to stabilize training and promote robust latent space construction. Extensive experiments conducted on state-of-the-art autoregressive frameworks, *e.g.*, LlamaGen [61] and RAR [84], across the ImageNet 256x256 generation benchmarks demonstrate the efficacy of our approach. Our proposed tokenizer, RobustTok, trained with latent perturbations, substantially outperforms existing methods, achieving notably lower gFID scores with accelerated convergence. Furthermore, through detailed ablation studies, we validate the effectiveness of perturbation parameters and

confirm that robustness gains directly translate to improved generative performance.

Our contribution can be summarized as follows.

- We conduct the first comprehensive analysis identifying insufficient robustness in discrete latent space as a primary factor leading to error accumulation in AR generative modeling.
- We propose perturbed FID (pFID), a novel evaluation metric explicitly designed to measure and correlate discrete latent space robustness with downstream generative modeling performance.
- We introduce RobustTok, a tokenizer trained using our plug-and-play perturbation approach that achieves superior performance in image generation benchmarks, significantly outperforming existing state-of-the-art methods.
- We provide extensive experiments and ablation studies to validate and analyze the effectiveness of latent perturbations in constructing robust discrete latent spaces.

2. Related Works

Image tokenizers. Image tokenization has seen significant advancements across various image-related tasks. Traditionally, autoencoders [21, 72] have been employed to compress images into latent spaces for downstream applications such as generation and understanding. In generative tasks, VAEs [52, 70] learn to map images to probabilistic distributions; VQGAN [15, 53] and its subsequent variants [23, 28, 40–42, 63, 76, 81–83, 88, 89, 91] introduce discrete latent spaces to enhance compression and facilitate the application of autoregressive models [14, 71] to image generation tasks by converting images into sequences of discrete tokens. On the other hand, understanding tasks, such as CLIP [51], DINO [9, 46, 92] and MAE [18], rely heavily on LLM [14, 71] to tokenize images into semantic representations [12, 45] where shown its promising performance in classification [14], object detection [90], segmentation [73], and multi-modal application [79]. For a long time, image tokenizer have been divided between methods tailored for generation and those optimized for understanding. Recently, multiple studies have demonstrated the feasibility of leveraging semantic information – traditionally used for understanding – in image generation, particularly within tokenization side. [35, 36, 80] integrate semantic information into the quantization process and demonstrated its effectiveness in the generative model. On the other hand, recent work [6, 7, 25, 86] leverages semantic information to mitigate information loss in the high-compression scenarios. In this paper, we provide a comprehensive analysis of image tokenizer in a view of perturbation robustness [5, 33, 34, 38, 39, 78].

Autoregressive visual generation. Pioneering work on autoregressive visual generation has shown remarkable suc-

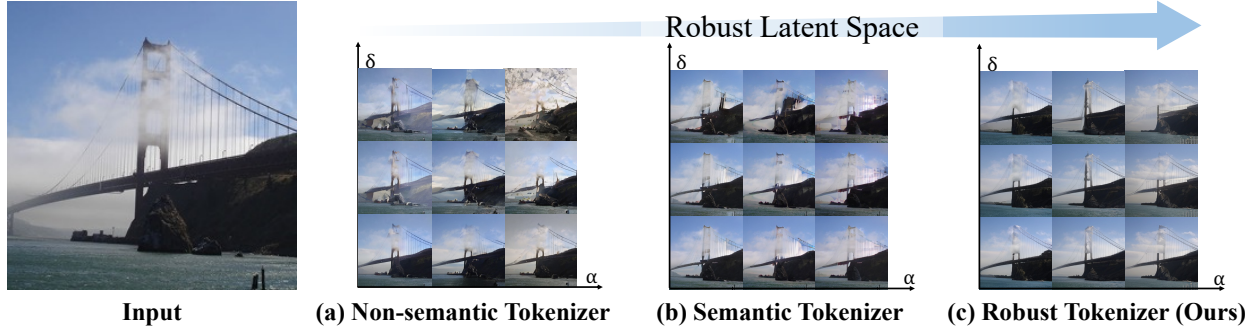


Figure 2. Visualization of (a) traditional tokenizer, (b) semantic tokenizer, and (c) our RobusTok in reconstruction task with Latent Perturbation. Non-semantic tokenizer leads to distorted reconstructions when perturbations are introduced while our method shows promising robustness to those perturbations.

cess in generating high-quality images by modeling the distribution of pixels or latent codes in a sequential manner. The autoregressive model, performed by RNNs [69], CNNs [68], and currently, Transformers [71], has demonstrated their strong capacity for capturing long-range dependencies and fine-grained details in image generation. Inspired by exploded development of language model [43, 59] such as GPT [1], a series of works leverage tokenizers to convert images or visual information into discrete latent codes, enabling autoregressive or MLM modeling to generate image in raster-scan [15] or parallel [4, 47, 74] order. Recently, autoregressive models continued to show their scalability power in larger datasets and multimodal tasks [19]; models like LlamaGen [61] and AiM [30] adapting current advanced LLM architectures for image generation. New directions such as VAR [17, 37, 50, 54, 64] and RAR [48, 84] focus on fusing global information into the training of autoregressive model and successfully achieve a promising result. MAR [32], Fluid [16], and GIVIT [66] have shown the potential for continuous image generation through autoregressive modeling. Based on the development of such, various technique are continue to unify the language language model for generation and understanding [65, 77].

3. Sampling Error Synthesis

Motivated by the AR improvement over semantic tokenization, we analyze the significance of sampling error during AR inference and propose a latent perturbation method for tokenizer training in this section.

3.1. Preliminaries

Vector Quantization (VQ). Most AR models are based on discrete tokenizers with a quantized latent space. The tokenizer usually consists of an encoder, a quantizer, and a decoder. Although many quantization techniques for the quantizer were previously proposed [41, 82, 87], we focus on the VQ tokenizer [15] for its simplicity and natural compatibility with AR models in this paper.

Given an RGB image I , the encoder \mathcal{E} first extracts a set of latent representations $Z \in \mathbb{R}^{H \times W \times C}$, where $H \times W$ denotes the spatial resolution of the latent tokens. VQ [15] aims to quantize continuous features into a set of discrete features Z' with a minimum reconstruction error of the original data, ensuring that the quantized representation remains as close as possible to the original continuous ones. Specifically, it maps each continuous feature vector $\mathbf{z} \in \mathbb{R}^C$ to a closest quantized codeword $\mathbf{e} \in \mathbb{R}^C$ from a learnable codebook $\mathcal{C} = \{\mathbf{e}_k\}_{k=1}^K$ with in total K codewords as:

$$\mathbf{z}' = \arg \min_{\mathbf{e}_k \in \mathcal{C}} \|\mathbf{z} - \mathbf{e}_k\|_2^2. \quad (1)$$

The decoder \mathcal{D} then reconstructs the original input signals by taking the quantized representation Z' as input.

Autoregressive Generation with VQ. Given a sequence of quantized tokens $Z' = \{\mathbf{z}'_1, \dots, \mathbf{z}'_T\}$ of length $T = H \times W$, AR models capture the entire distribution as:

$$p(\mathbf{z}'_1, \dots, \mathbf{z}'_T; \theta) = \prod_{t=1}^T p(\mathbf{z}'_t | \mathbf{z}'_{<t}; \theta), \quad (2)$$

where θ represents the parameters of a deep neural network. To learn the network, AR models are trained to predict the tokens at timestep/position t , given all the preceding ground truth tokens, known as teacher forcing [62]. However, this mechanism introduces a discrepancy in the inference stage, where, during AR inference, the predicted tokens are conditioned on the preceding predictions instead of the ground truth ones. This discrepancy can introduce and then accumulate errors during inference, resulting in generations of degraded quality [3, 26].

3.2. Latent Perturbation

Knowing that AR models are subjected to sampling error accumulation due to the discrepancy between training and inference, we show in the following that such sampling error of AR models can be captured within the tokenizer alone

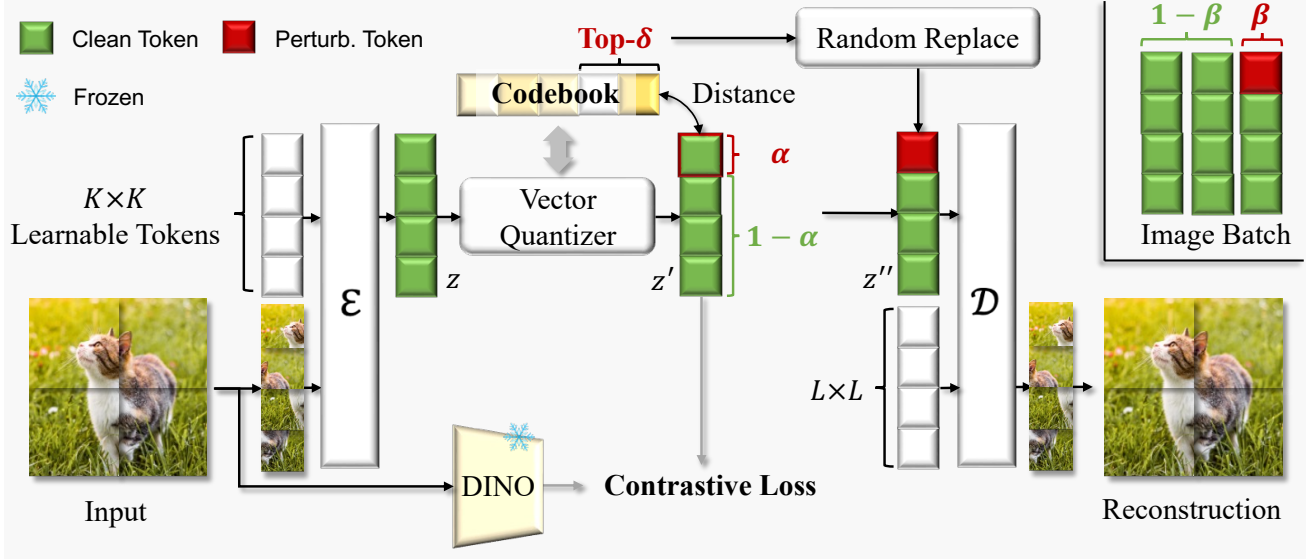


Figure 3. RobustTok overview. We adopt vision transformer as our encoder \mathcal{E} and decoder \mathcal{D} . β of data in one batch will process our Latent Perturbation, which will be randomly replaced by top- δ neighbor from codebook with probability α . A frozen DINO encoder is utilized to supervise our latent space.

with a novel reconstruction metric, and can be mitigated by involving perturbation into tokenizer training in a plug-and-play manner. More specifically, we can simulate the sampling error, *i.e.*, unexpected tokens during sampling of AR models, with perturbed latent tokens and to enhance the robustness of the tokenizer, as shown in Fig. 2.

Perturbation rate. An important metric to monitor the AR modeling process is the accuracy of predicted tokens. Likewise, we define a perturbation rate α to control the proportion of perturbed token within an image. Given the quantized feature $Z' \in \mathbb{R}^{H \times W \times C}$, we define α as:

$$\alpha = \frac{P}{H \times W}, \quad (3)$$

where P denotes the perturbed token number. To simulate the sampling error, we can randomly perturb the quantized tokens from the tokenizer encoder.

Perturbation proportion. Within a batch of images, we apply the perturbation in a proportion β of images and keep the remaining images unchanged. With N_c clean images and N_p perturbed images, the perturbation proportion is calculated as:

$$\beta = \frac{N_c}{N_c + N_p}. \quad (4)$$

Perturbation strength. We define a perturbation strength δ to quantify the perturbation level. Specifically, given a discrete token $\mathbf{z} = \mathbf{e}_k$ with a codebook \mathcal{C} , we calculate the

| Ideal Scenario | Train Tokenizer | Eval AR/LLM |
|-------------------------------|-------------------------------------|---|
| $\mathcal{D}(\mathbf{z}) = I$ | $\mathcal{D}(\mathbf{z}) = \hat{I}$ | $\mathcal{D}(\mathbf{z} + \Delta) = \hat{I}'$ |

Table 1. Decoder analysis. I : input image. \hat{I} : predicted image. \hat{I}' : predicted image from noisy latent. \mathbf{z} : latent feature. Δ : sampling error. \mathcal{D} : decoder.

set of top- δ nearest neighbors:

$$\mathcal{S}_\delta = \arg \min_{\mathcal{S}_\delta \subset \mathcal{C}, |\mathcal{S}_\delta| = \delta} \sum_{\mathbf{e}_n \in \mathcal{S}_\delta} \|\mathbf{e}_n - \mathbf{e}_k\|_2^2, \quad (5)$$

where $|\cdot|$ denotes the counting operation. We randomly replace the original token \mathbf{e}_k with a $\mathbf{e}_\delta \in \mathcal{S}_\delta$ to perturb the latent, thereby modifying the latent representation to simulate sampling in AR with the top- k nucleus strategy.

3.3. Robustness Indicator: Perturbed FID

Analysis - Lipschitz smoothness. We analyze the discrepancy between tokenizer training and inference schemes. As shown in Tab. 1, we demonstrate the input/output formulation of visual decoder upon the latent representations \mathbf{z} . Ideally, the decoder \mathcal{D} should take a clear latent \mathbf{z} and reconstruct the input image I that aligns with the current tokenizer training target. However, during the inference stage with a well-trained AR/LLM, sampling error Δ always happens. This will change the usage of the decoder differently from its training target, which significantly challenges the robustness of the visual decoder during inference as we expect $\mathcal{D}(\mathbf{z} + \Delta)$ can still reconstruct the input I . The decoder's robustness can be measured by the Lipschitz smoothness $Lip = \frac{\hat{I}' - \hat{I}}{\Delta} \approx \frac{\hat{I}' - I}{\Delta}$. However, in a discrete

| Codebook Size | Method | Tokenizer Type | Tokenizer | | Generator | |
|---------------|------------------|-------------------|-------------|-------------|-------------|-------------|
| | | | rFID↓ | pFID↓ | gFID↓ | gFID↓ (CFG) |
| 16384 | VQGAN-16384 [15] | Non-semantic | 4.50 | 18.18 | 37.39 | 14.80 |
| | LlamaGen [61] | Non-semantic | 2.19 | 13.12 | 26.34 | 8.61 |
| | IBQ-16384 [58] | Non-semantic | 1.41 | 16.35 | 30.19 | 11.01 |
| | VQGAN-LC [89] | Semantic* | 3.27 | 16.78 | 31.35 | 11.80 |
| 8192 | IBQ-8192 [58] | Non-semantic | 1.87 | 19.62 | 30.91 | 10.85 |
| | TiTok [85] | Semantic | 1.03 | 3.55 | 25.66 | 8.84 |
| | XQGAN-8192 [36] | Semantic | 0.81 | 7.91 | 25.43 | 10.18 |
| 4096 | XQGAN-4096 [36] | Semantic | 0.91 | 6.98 | 13.58 | 6.91 |
| | RobustTok (Ours) | Semantic + Robust | 1.02 | 2.28 | 9.47 | 5.67 |
| 1024 | MaskGIT [4] | Non-Semantic | 2.28 | 4.20 | 18.02 | 5.85 |
| | IBQ-1024 [58] | Non-Semantic | 2.24 | 6.37 | 35.33 | 11.01 |

Table 2. Benchmark of tokenizers with the same LlamaGen-B generator. For fair comparison, the gFID with classifier-free guidance utilizes the same classifier value and schedule. All the tokenizers share the same $C \times 16 \times 16$ latent shape. We discuss the reason of choosing codebook size 4096 to train RobustTok in the ablation. More benchmarking results with larger generators are available in the appendix. * denotes semantics captured with linear projection. All metrics, *i.e.*, rFID, pFID and gFID, are the smaller the better.

latent space, the potential choice of Δ is constrained and the discrepancy between input I and reconstructed images \hat{I} can be better reflected by the Fréchet Inception Distance (FID). In this way, we introduce perturbed FID (pFID) as a new metric to reflect the robustness and reconstruction quality of image tokenizers.

Perturbed FID. With the latent perturbation parameters: α , β and δ , we propose a novel reconstruction metric, termed as Perturbed FID (pFID). Compared to reconstruction FID (rFID) that merely captures the reconstruction quality of the tokenizer, pFID can reflect the robustness and the latent space from a tokenizer, and correlates with the sampling error and thus the performance of AR models.

To calculate the pFID, we apply perturbation among all images, *i.e.*, $\beta = 1$ for all the settings. In addition, to simulate different noisy level during inference, we define a set of perturbation rates $\alpha \in \{0.9, 0.8, 0.7, 0.6, 0.5\}$ and a set of perturbation strength $\delta \in \{200, 280, 360\}$. Combining both sets, we have a total of 15 combinations of perturbation settings. We generate images with all settings and calculate the FID between input images. The averaged value serves as pFID. Specifically, the perturbation strength is linearly scaled to adopt different codebook sizes.

We present a comparison of rFID and pFID in Fig. 4, and provide more analysis on the results in Sec. 4.2. To summarize, our pFID is more correlated with the tokenizer’s downstream generation performance compared with rFID.

3.4. RobustTok

Inspired by the proposed pFID metric, which shows the robustness of the discrete latent space is important to capture the sampling error of AR models, we demonstrate that we can further involve such perturbation into tokenizer training to proactively learn a more robust latent space.

Architecture. Following prior works [35, 36, 85], RobustTok leverages Vision Transformer (ViT) [13] as visual encoder and visual decoder. As shown in Fig. 3, we initialize a set of learnable tokens and use these tokens as the representation for image reconstruction and subsequent generation. Specifically, the input image is first patchified to $L \times L$ tokens, where L represents the patch size, and concatenated with learnable tokens to serve as the input of the encoder. We apply vector quantization on the continuous token z obtained from the encoder \mathcal{E} . After that a latent perturbation approach is applied to guide the latent space construction. Finally, the ViT decoder takes perturbed tokens z'' and a new set of learnable tokens to reconstruct the image. Specifically, we incorporate a pretrained DINOv2 model [46] to inject semantics, ensuring that the learned tokens retain meaningful visual semantics and structural coherence.

Plug-and-play perturbation. During tokenizer training, we apply latent perturbation to enhance its robustness. We apply perturbation after semantic regularization [35] to preserve clear semantics in the discrete tokens to maximize the reconstruction capability. Within a batch of image, we

| Type | Method | Tokenizer | | Generator | | | | | | |
|------------------------|------------------------|-----------|-------|-----------|-------|------|------|-------|-------|------|
| | | rFID↓ | pFID↓ | gFID↓ | IS↑ | Pre↑ | Rec↑ | #Para | Leng. | Step |
| Diff. | ADM [11] | - | - | 10.94 | 101.0 | 0.69 | 0.63 | 554M | - | 1000 |
| | LDM-4 [56] | - | - | 3.60 | 247.7 | - | - | 400M | - | 250 |
| | DiT-L/2 [49] | 0.90 | - | 5.02 | 167.2 | 0.75 | 0.57 | 458M | - | 250 |
| | MAR-B [32] | 1.22 | - | 2.31 | 281.7 | 0.82 | 0.57 | 208M | - | 64 |
| NAR | MaskGIT [4] | 2.28 | 5.03 | 6.18 | 182.1 | 0.80 | 0.51 | 227M | 256 | 8 |
| | RCG (cond.) [31] | - | - | 3.49 | 215.5 | - | - | 502M | 256 | 250 |
| | TiTok-S-128[85] | 1.52 | - | 1.94 | - | - | - | 177M | 128 | 64 |
| | MAGVIT-v2 [82] | 0.90 | - | 1.78 | 319.4 | - | - | 307M | 256 | 64 |
| | MaskBit [76] | 1.51 | - | 1.65 | 341.8 | - | - | 305M | 256 | 64 |
| AR | VQGAN [15] | 7.94 | - | 18.65 | 80.4 | 0.78 | 0.26 | 227M | 256 | 256 |
| | RQ-Transformer [29] | 1.83 | - | 15.72 | 86.8 | - | - | 480M | 1024 | 64 |
| | LlamaGen-L [61] | 2.19 | 13.12 | 3.80 | 248.3 | 0.83 | 0.52 | 343M | 256 | 256 |
| | VAR [64] | 0.90 | 17.46 | 3.30 | 274.4 | 0.84 | 0.51 | 310M | 680 | 10 |
| | ImageFolder [64] | 0.80 | 7.23 | 2.60 | 295.0 | 0.75 | 0.63 | 362M | 286 | 10 |
| | RAR-B [84] | 2.28 | 5.03 | 1.95 | 290.5 | 0.82 | 0.58 | 261M | 256 | 256 |
| | RAR-L [84] | - | - | 1.70 | 299.5 | 0.81 | 0.60 | 461M | 256 | 256 |
| | RobustTok-RAR-B (Ours) | 1.02 | 2.28 | 1.83 | 298.3 | 0.80 | 0.63 | 261M | 256 | 256 |
| RobustTok-RAR-L (Ours) | - | - | 1.60 | 305.8 | 0.78 | 0.65 | 461M | 256 | 256 | |

Table 3. System-level performance comparison on class-conditional ImageNet 256x256. \uparrow and \downarrow indicate that higher or lower values are better, respectively.

randomly choose β of them to add perturbation. To apply perturbation to each selected image, we randomly choose $\alpha \times H \times W$ tokens and then calculate the top- δ nearest neighbors to those tokens within the learned codebook. The final perturbation is applied by randomly replacing the original token with its top- δ nearest neighbor.

4. Experiment

4.1. Experimental Setting

We experiment on 256×256 ImageNet [10] benchmark for both reconstruction and generation. As summarized in Tab. 2, we first evaluate 11 popular tokenizers across 4 codebook sizes. This almost includes all open-sourced discrete tokenizers. The usage of all off-the-shelf tokenizers follows their official implementation and pre-trained weights. We pre-tokenize images with pre-trained tokenizers and benchmark their generation performance using LlamaGen-Base/Large generators with default settings [61]. For RobustTok, we additionally leverage RAR [84] as an additional generator to validate its wide applicability.

Evaluation metric. We employ Fréchet Inception Distance (FID) [20], Inception Score (IS) [57], Precision, and Recall as metrics to assess generation quality. We report the results of both using classifier-free guidance (CFG) [22] and without using CFG. For tokenizer, we utilize rFID and pFID to evaluate tokenizer reconstruction quality and robustness.

Implementation details. RobustTok follows the XQGAN [36] training setting but replaces product quantization with vanilla vector quantization [35]. We retain semantic regularization to stabilize the latent space. During tokenizer training, we randomly select $\beta = 0.1$ of the total data to add perturbation. For these selected samples, we set $\alpha = 1.0$ and $\delta = 100$, and gradually anneal to half over the training. For the AR generator, we strictly follow the training recipes of LlamaGen [61] and RAR [84] except for changing the tokenizer to RobustTok.

4.2. Result Analysis

Generic take-home observations. Before we go through and validate the core focus of this paper, we aim to conclude some generic observations from the benchmarking. The observations are summarized from the benchmarking results of LlamaGen-Base/Large.

- **Codebook size:** With similar reconstruction capability, the smaller the codebook size, the better the generation quality. We consider this property primarily results from the simple latent space are easier to capture during the AR modeling.
- **Semantics:** Semantic tokenizer typically demonstrates better capability for both reconstruction and generation. Semantic guidance provides a structural and clustering latent for better compression capability for reconstruction and robustness property for generation accordingly.
- **Reconstruction:** Reconstruction capability measured by traditional rFID does not align with the generation capability. This should be potentially resulted from the dis-

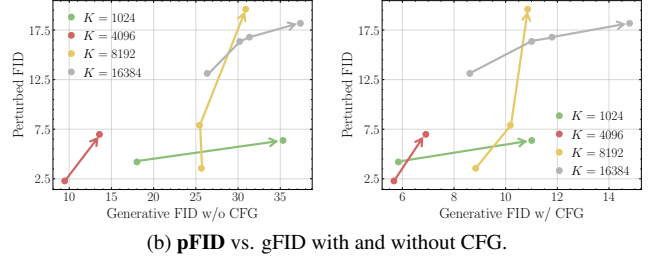
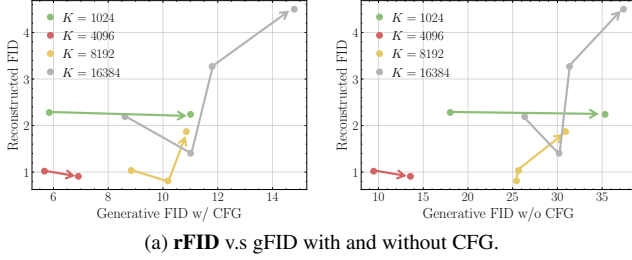


Figure 4. Comparison of rFID-gFID and pFID-gFID curves of different tokenizers under LlamaGen-B training setting. K denotes codebook size. Each point represents a method in Tab. 2.

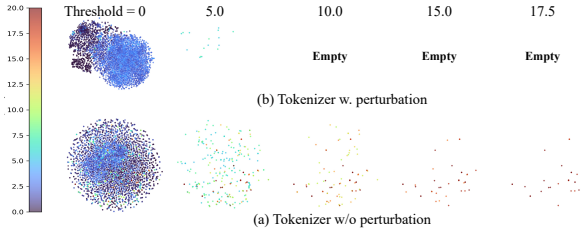


Figure 5. T-SNE visualization of latent space of tokenizer trained with and without latent perturbation. Colors and thresholds represent the frequency of tokens being used during inference without perturbation.

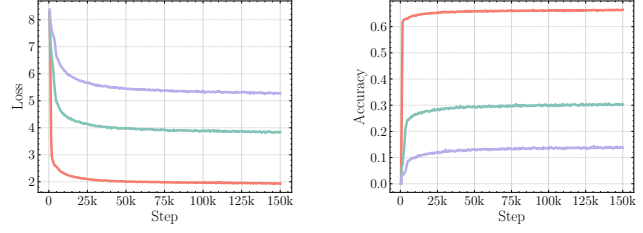


Figure 6. RAR training curve for **None**, **Half**, and **Zero** annealing strategies. The tokenizer without annealing exhibits strong convergence but compromises diversity, while annealing to zero offers limited improvement over the baseline.

crepancy between tokenizer training and inference, *i.e.*, the latent space lacks robustness.

Effectiveness of pFID. To better compare the correlation among metrics, we visualize the rFID-gFID and pFID-gFID curves as shown in Fig. 4 (more results with the LlamaGen-Large generator are available in the Appendix). (a) When comparing rFID and gFID, we observe that there is no clear correlation between them, regardless of whether classifier-free guidance is used in generation or not. (b) Differently, pFID and gFID demonstrate a strong correlation within each codebook size K . We separately compare results within each K primarily because we add different perturbation strength δ according to K . With the new pFID, we can better access the tokenizer’s performance without the time-consuming and resource-intensive training of subsequent generators.

Systematic comparison. As shown in Tab. 3, we compare our RobustTok with various state-of-the-art methods on the ImageNet 256x256 [10] benchmark. Notably, our proposed RobustTok leads to a significant improvement over previous methods. Specifically, 0.12 and 0.10 gFID gains are achieved by utilizing RobustTok on top of RAR generator. And finally, with a 461M model, our approach achieves a 1.60 gFID.

| Method | rFID↓ | pFID↓ | gFID↓ w/o. CFG | CFG |
|----------------------|-------|-------|-------------------|------|
| <i>LlamaGen-L</i> | | | | |
| XQGAN [36] | 0.81 | 7.91 | 14.64 | 4.48 |
| + $K = 4096$ | 0.91 | 6.98 | 7.91 | 4.13 |
| + L.P. $\beta = 0.5$ | 3.97 | 4.52 | 9.31 | 5.40 |
| + L.P. $\beta = 0.1$ | 1.58 | 3.61 | 4.60 | 3.93 |
| <i>RAR-B</i> | | | | |
| + L.P. $\mapsto 0$ | 0.97 | 4.89 | 5.32 | 1.97 |
| + L.P. $\mapsto 0.5$ | 1.02 | 2.28 | 4.62 | 1.85 |

Table 4. Ablation of RobustTok. L.P. stands for our proposed Latent Perturbation. $\mapsto 0/0.5$ denotes annealing the perturbation to none and half respectively. gFID with classifier-free guidance (CFG) uses the constant schedule for LlamaGen and the linear schedule for RAR.

Robust latent space. As shown in Fig. 5, we compare the latent space (*i.e.*, codebook) with and without latent perturbation. We colorize the latent tokens with their frequency of use during inference. When truncating tokens at different usage count thresholds, we observe the space constructed with latent perturbation contains many reusable tokens, which acted as key tokens that can be easily modeled, while the remaining tokens serve as supportive tokens providing finer detailed information. In contrast, the latent space without latent perturbation distributes usage more uniformly across tokens.

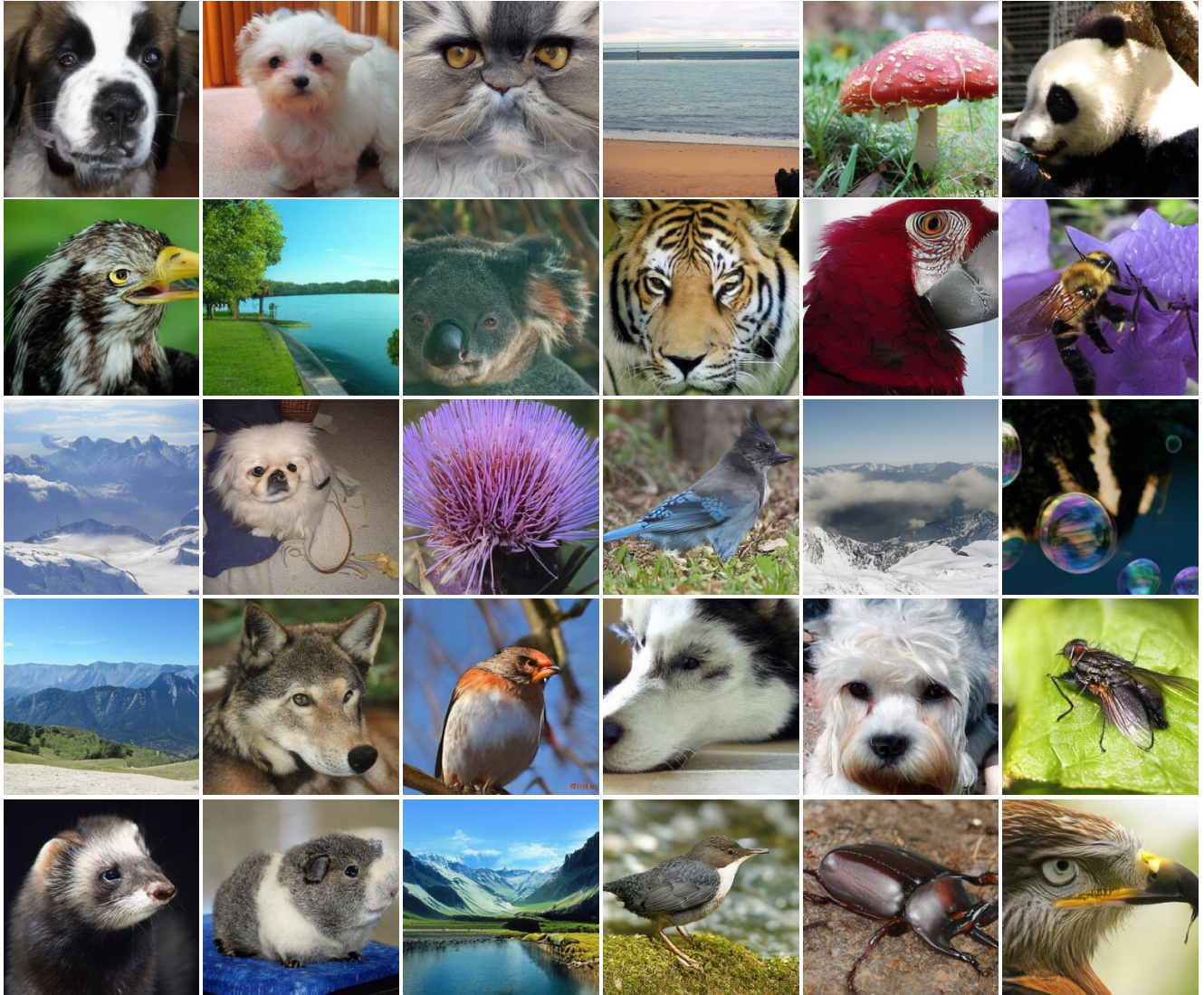


Figure 7. Visualization of 256×256 image generation within ImageNet class.

Perturbation selection & annealing strategy. As shown in Tab. 4, we conduct an ablation to determine the optimal selection of perturbation hyperparameters. Our results indicate that using a large perturbation parameter, *e.g.*, $\beta = 0.5$, degrades the model’s reconstruction capability and adversely affects generative performance. Furthermore, training without annealing strategy leads to mode collapse and loss of generation diversity, whereas annealing to zero results in an overly deterministic tokenizer, diminishing the flexibility observed in Fig. 5. We find that annealing to half strikes a balance between robustness and adaptability, preserving essential latent properties while improving the quality of generated outputs. We show the loss curves and accuracy of predicted tokens during training in Fig. 6.

Qualitative results. We demonstrate images generated by our approach as shown in Fig. 7.

5. Conclusion

Limitation. Though we focus on a discrete latent space in this paper, the discussed problem also exists in continuous tokenizers with diffusion models. However, the latent perturbation (*e.g.*, non-scheduled noise) in continuous tokenizer is more challenging to determine as the perturbation is not constrained by a codebook. We leave this as future work.

In this paper, we introduce RobustTok, a novel tokenizer training scheme designed to enhance the robustness of discrete latent spaces in autoregressive image generation. Through our proposed latent perturbation approach, we successfully address the issue of error accumulation that arises from discrepancies between training and inference conditions. Furthermore, we introduced Perturbed FID (pFID), a new metric that effectively correlates tokenizer robustness

| Cluster Number | 512 | 1024 | 2048 | 4096 | 8192 | 16384 | | | | | |
|----------------|------|------|------|------|------|-------|------|-----|------|-----|------|
| SSE. | 2250 | 1637 | -613 | 1253 | -384 | 928 | -325 | 611 | -317 | 473 | -138 |

Table A. K-means clustering analysis of DINO features in ImageNet validation set. SSE. denotes as the Sum of Squared Error. The subscript values represent the difference in SSE. relative to the previous cluster number, indicating the reduction in error as the number of clusters increases.

with downstream generative quality, bridging the gap between reconstruction-focused evaluation and actual generation performance. We hope this research can provide the community with a new direction in designing effective tokenizers for generation models.

A. Appendix

A.1. Codebook Size Selection

As described in ablation, we initialize our tokenizer with XQGAN-8192 [36]. Motivated by insights from [76, 84] and our own benchmarking, we aim to reduce the codebook size for a more compact representation while preserving high reconstruction fidelity and generative quality. However, as shown in Fig. B, the latent space of images in XQGAN-1024 appears highly fragmented, resulting in notable robustness discrepancies compared to tokenizers with larger codebooks, such as XQGAN-8192 and XQGAN-16384.

To better understand this, we analyze DINO features on ImageNet and apply k-means clustering to feature embeddings. As shown in Tab. A, the results of the clustering of k-means, evaluated using the elbow method, indicate decreasing improvements in the Sum of Squared Errors (SSE) as the number of clusters increases beyond 4096. The reduction in SSE slows significantly at this point, suggesting that further increasing the number of clusters yields only marginal benefits. Based on this observation, we select $K = 4096$ as the codebook size for our tokenizer.

A.2. Loss Function.

The RobustTok is trained with composite losses including reconstruction loss \mathcal{L}_{recon} , vector quantization loss \mathcal{L}_{VQ} [15], adversarial loss \mathcal{L}_{ad} [24], Perceptual loss \mathcal{L}_P [27], and semantic loss \mathcal{L}_{clip} [35]:

$$\mathcal{L} = \lambda_{rec}\mathcal{L}_{rec} + \lambda_{VQ}\mathcal{L}_{VQ} + \lambda_{ad}\mathcal{L}_{ad} + \lambda_P\mathcal{L}_P + \lambda_{sem}\mathcal{L}_{sem}. \quad (6)$$

Specifically, the reconstruction loss measures the L_2 distance between the reconstructed image and the ground truth; vector quantization loss encourages the encoded features and its aligned codebook vectors; adversarial loss ensures that the generated images are indistinguishable from real ones; perceptual loss compares high-level feature representations to capture structural differences; and semantic loss performs semantic regularization between semantic tokens and the pre-trained DINOv2 [46] features.

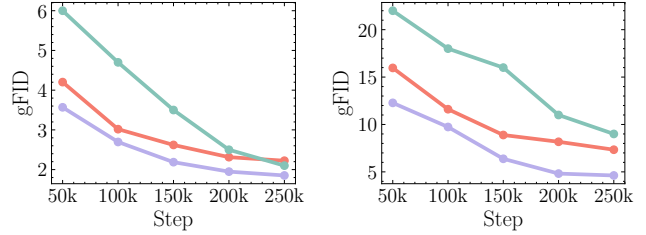


Figure A. Visualization of gFID trends for RAR, XQGAN, and Ours with (left) and without (right) CFG.

DINO supervision. As shown in Fig. C, we visualize the means of DINO pixel features (Fig. Ca) and DINO class features (Fig. Cb). We observe that DINO class features exhibit a more structured representation compared to pixel-level features, which appear to be more scattered. Since the purpose of DINO features in our model is to provide supervision, the structured nature of class features makes them a more suitable choice to guide the learning process.

A.3. RAR Training

We follow the RAR training setting to validate the performance of our RobustTok. Specifically, as shown in Fig. A, we evaluate RAR, XQGAN(our baseline), and our proposed RobustTok during training. We observe that XQGAN achieves a faster convergence speed and better performance without CFG; however, its final performance, with a gFID of 2.22 under classifier-free guidance (CFG), remains sub-optimal compared to RAR. Our RobustTok, inheriting the structural advantages of the semantic tokenizer while incorporating a robust latent space, not only achieves faster convergence but also outperforms both XQGAN and vanilla RAR in final generative quality, demonstrating its effectiveness in preserving semantic consistency and enhancing feature representation. This highlights a promising direction for designing more robust training schemes to further improve generative performance.

A.4. Latent Perturbation v.s. Other Noises

To avoid potential misunderstanding, we aim to discuss the difference between our proposed latent perturbation and other noises used in generative models.

- **Latent perturbation:** Latent perturbation is a **random** noise manually added to the latent space based on the pattern we observed during the real sampling errors. Specifically, it is added in a cluster-based manner enlarging the decision boundary and zero-shot generalization during inference.
- **Diffusion noise:** Diffusion noise is a **scheduled** noise added to enable the reverse process using a diffusion sampler. It follows a pre-defined schedule to systematically disrupt the latent space.

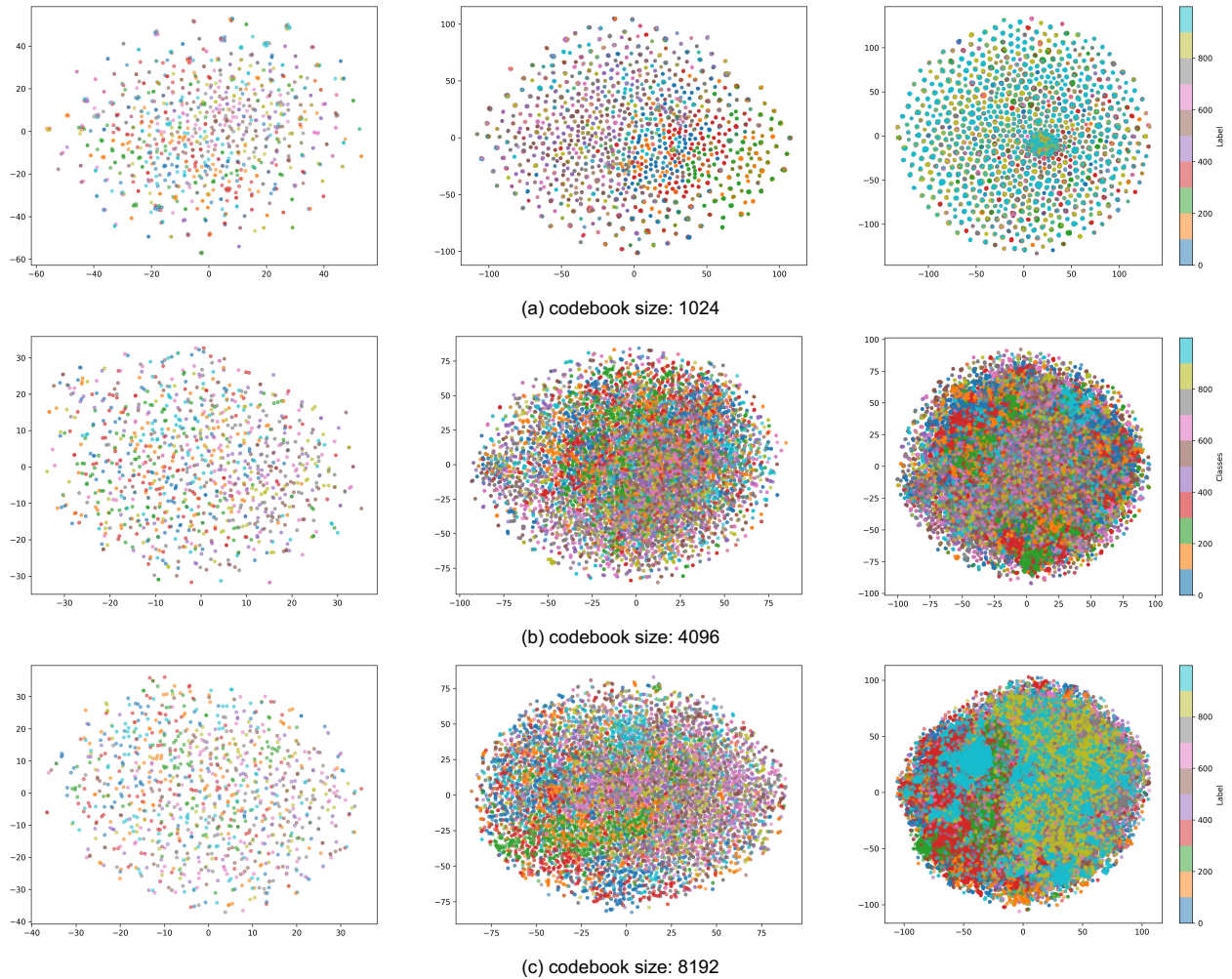


Figure B. T-SNE visualization of latent space in XQGAN with varying codebook sizes setting: (a) 1024, (b) 4096, and (c) 8192. Each subfigure presents embeddings derived from (left) 1,000, (middle) 10,000, and (right) 50,000 samples from the ImageNet validation set. Compared to larger codebook sizes, XQGAN-1024 fails to maintain a well-structured latent space, leading to increased fragmentation and reduced robustness.

- **Gaussian noise in VAE:** VAE's reparameterization employs a gaussian noise to decompose the mean value and randomness of the distribution to enable the gradient backpropagation.

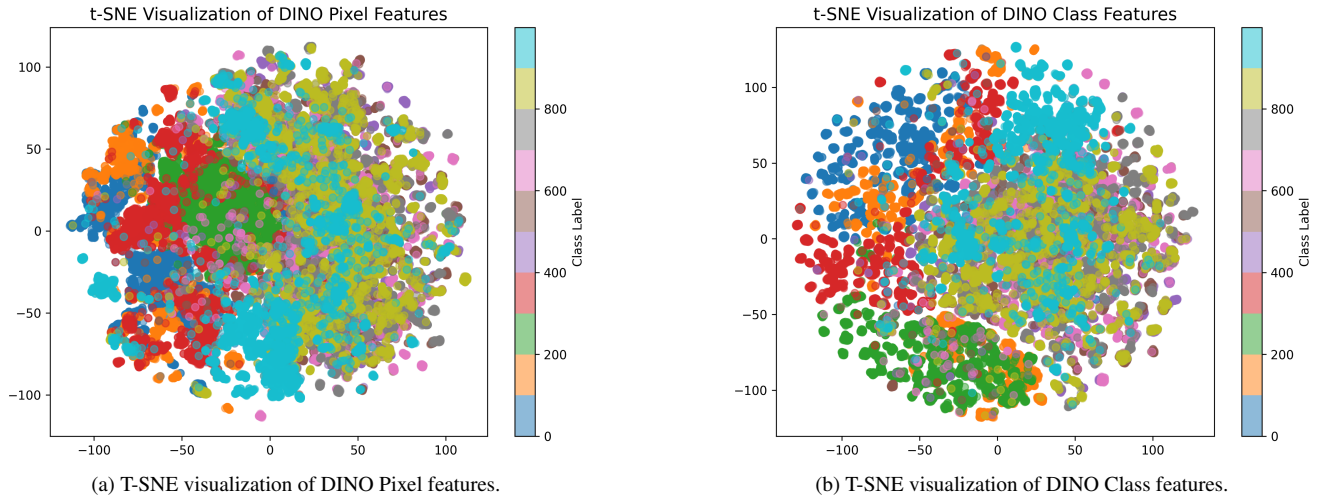


Figure C. Visualization of DINO features in ImageNet Validation Set.

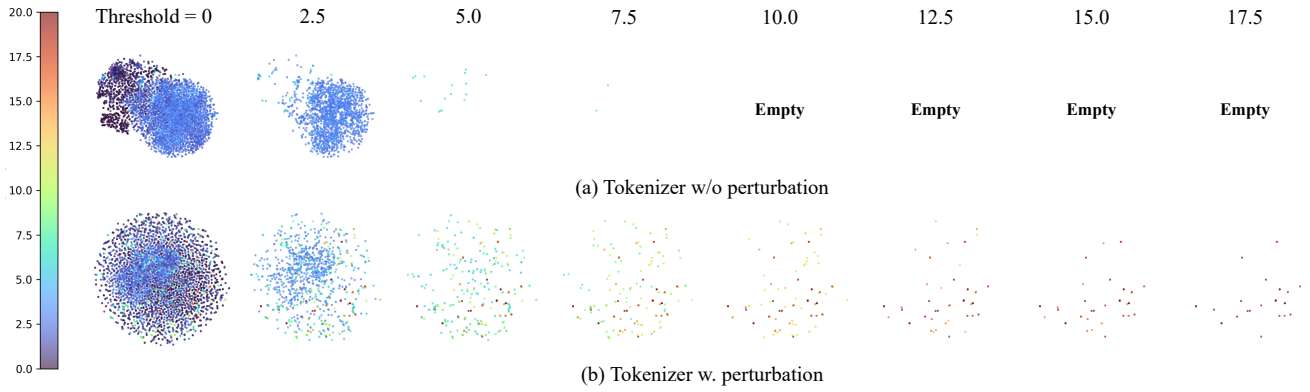
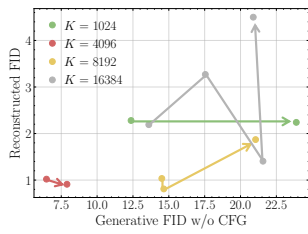


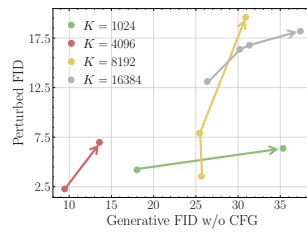
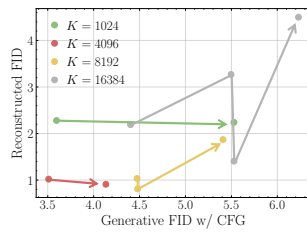
Figure D. Detailed t-SNE visualization of latent space of tokenizer training with and without our proposed latent perturbation.

| Codebook Size | Method | Tokenizer Type | Tokenizer | | Generator | |
|---------------|-------------------------|--------------------------|-------------|-------------|-------------|-------------|
| | | | rFID | pFID | gFID | gFID (CFG) |
| 16384 | VQGAN-16384 [15] | Non-semantic | 4.50 | 18.18 | 20.89 | 6.23 |
| | LlamaGen [61] | Non-semantic | 2.19 | 13.12 | 8.61 | 4.40 |
| | IBQ-16384 [58] | Non-semantic | 1.41 | 16.35 | 21.57 | 5.53 |
| | VQGAN-LC [89] | Trainable Projector | 3.27 | 16.78 | 17.55 | 5.50 |
| 8192 | IBQ-8192 [58] | Non-semantic | 1.87 | 19.62 | 21.05 | 5.41 |
| | TiTok [85] | Semantic | 1.03 | 3.55 | 14.51 | 4.47 |
| | XQGAN-8192 [36] | Semantic | 0.81 | 7.91 | 14.64 | 4.48 |
| 4096 | XQGAN-4096 [36] | Semantic | 0.91 | 6.98 | 7.90 | 4.13 |
| | RobustTok (Ours) | Semantic + Robust | 1.02 | 2.28 | 6.47 | 3.51 |
| 1024 | MaskGIT [4] | Non-Semantic | 2.28 | 4.20 | 12.37 | 3.60 |
| | IBQ-1024 [58] | Index Non-Semantic | 2.24 | 6.37 | 23.89 | 5.53 |

Table B. Tokenizer benchmarking for LlamaGen-L. All metrics, *i.e.*, rFID, pFID and gFID, are the smaller the better.



(a) **rFID** v.s gFID with and without CFG.



(b) **pFID** vs. gFID with and without CFG.

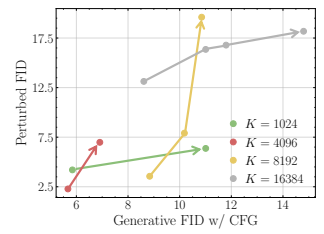
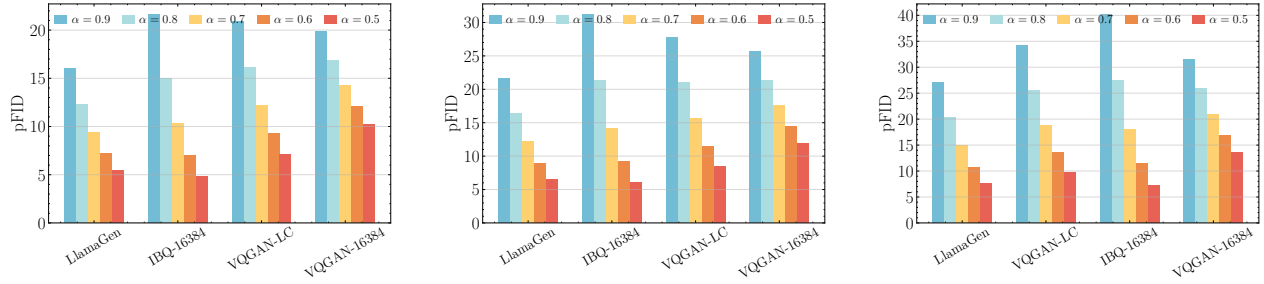
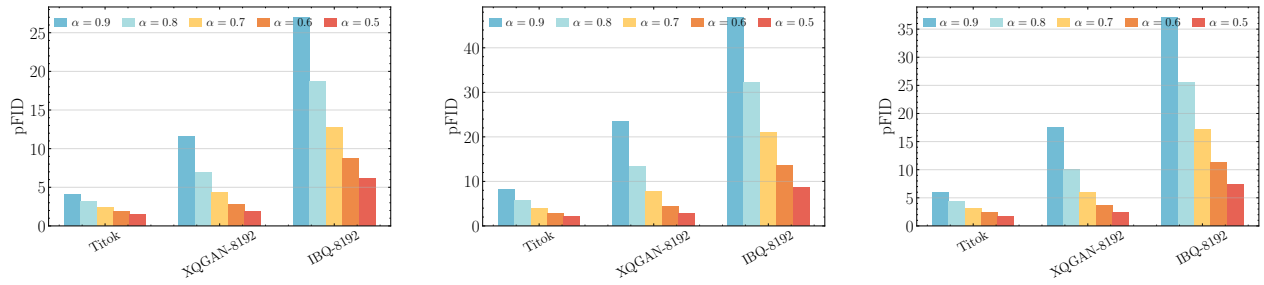


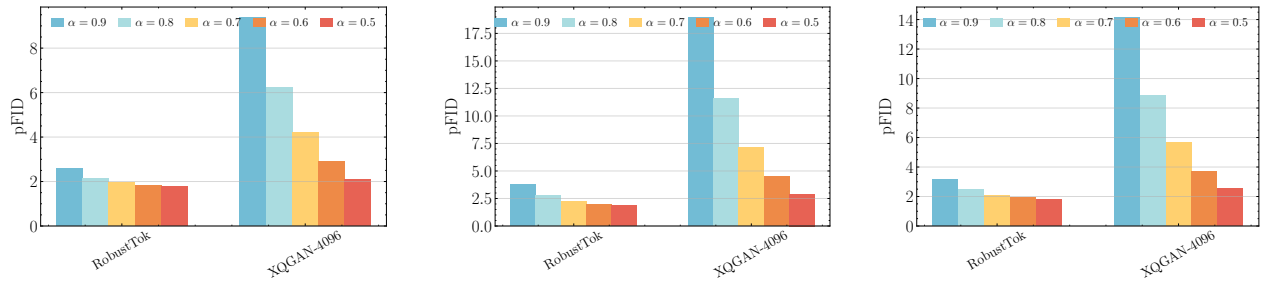
Figure E. Comparison of reconstructed FID relation to generative FID with perturbed FID relation to generative FID. All generators follow LlamaGen-L training setting. K denotes as codebook size.



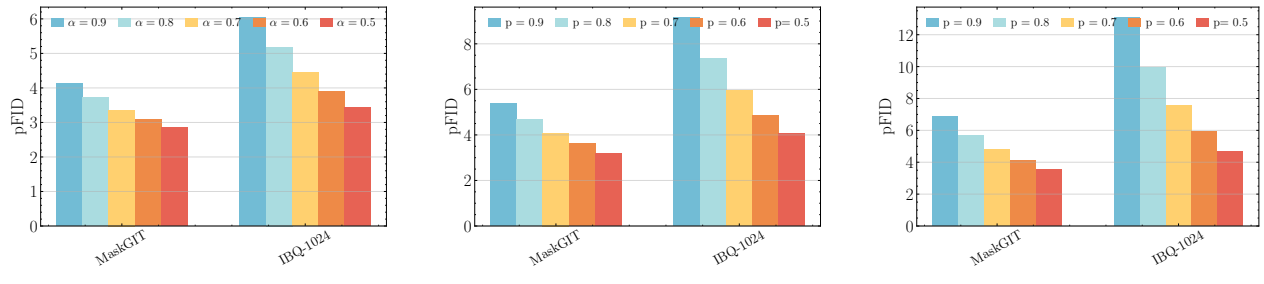
(a) Perturbed FID in Tokenizer with 16384 codebook in $\delta = \{200, 280, 360\}$



(d) Perturbed FID in Tokenizer with 8192 codebook in $\delta = \{100, 140, 180\}$



(c) Perturbed FID in Tokenizer with 4096 codebook in $\delta = \{50, 70, 90\}$



(d) Perturbed FID in Tokenizer with 1024 codebook in $\delta = \{10, 15, 20\}$

Figure F. qualitative analysis of tokenizers in our latent perturbation.

References

- [1] Josh Achiam, Steven Adler, Sandhini Agarwal, Lama Ahmad, Ilge Akkaya, Florencia Leoni Aleman, Diogo Almeida, Janko Altenschmidt, Sam Altman, Shyamal Anadkat, et al. Gpt-4 technical report. *arXiv preprint arXiv:2303.08774*, 2023. 1, 3
- [2] Roman Bachmann, Jesse Allardice, David Mizrahi, Enrico Fini, Oğuzhan Fatih Kar, Elmira Amirloo, Alaaeldin El-Nouby, Amir Zamir, and Afshin Dehghan. Flextok: Resampling images into 1d token sequences of flexible length. *arXiv preprint arXiv:2502.13967*, 2025. 1
- [3] Samy Bengio, Oriol Vinyals, Navdeep Jaitly, and Noam Shazeer. Scheduled sampling for sequence prediction with recurrent neural networks. *Advances in neural information processing systems*, 28, 2015. 3
- [4] Huiwen Chang, Han Zhang, Lu Jiang, Ce Liu, and William T. Freeman. Maskgit: Masked generative image transformer, 2022. 3, 5, 6, 11
- [5] Hao Chen, Yujin Han, Diganta Misra, Xiang Li, Kai Hu, Difan Zou, Masashi Sugiyama, Jindong Wang, and Bhiksha Raj. Slight corruption in pre-training data makes better diffusion models. *arXiv preprint arXiv:2405.20494*, 2024. 2
- [6] Hao Chen, Ze Wang, Xiang Li, Ximeng Sun, Fangyi Chen, Jiang Liu, Jindong Wang, Bhiksha Raj, Zicheng Liu, and Emad Barsoum. Softvq-vae: Efficient 1-dimensional continuous tokenizer. *arXiv preprint arXiv:2412.10958*, 2024. 2
- [7] Hao Chen, Yujin Han, Fangyi Chen, Xiang Li, Yidong Wang, Jindong Wang, Ze Wang, Zicheng Liu, Difan Zou, and Bhiksha Raj. Masked autoencoders are effective tokenizers for diffusion models. *arXiv preprint arXiv:2502.03444*, 2025. 1, 2
- [8] Chung-Cheng Chiu, Tara N Sainath, Yonghui Wu, Rohit Prabhavalkar, Patrick Nguyen, Zhifeng Chen, Anjali Kannan, Ron J Weiss, Kanishka Rao, Ekaterina Gonina, et al. State-of-the-art speech recognition with sequence-to-sequence models. In *2018 IEEE international conference on acoustics, speech and signal processing (ICASSP)*, pages 4774–4778. IEEE, 2018. 1
- [9] Timothée Darcet, Maxime Oquab, Julien Mairal, and Piotr Bojanowski. Vision transformers need registers, 2023. 2
- [10] Jia Deng, Wei Dong, Richard Socher, Li-Jia Li, Kai Li, and Li Fei-Fei. Imagenet: A large-scale hierarchical image database. In *2009 IEEE conference on computer vision and pattern recognition*, pages 248–255. Ieee, 2009. 6, 7
- [11] Prafulla Dhariwal and Alex Nichol. Diffusion models beat gans on image synthesis, 2021. 1, 6
- [12] Xiaoyi Dong, Jianmin Bao, Ting Zhang, Dongdong Chen, Weiming Zhang, Lu Yuan, Dong Chen, Fang Wen, Nenghai Yu, and Baining Guo. Peco: Perceptual codebook for bert pre-training of vision transformers. In *Proceedings of the AAAI Conference on Artificial Intelligence*, pages 552–560, 2023. 2
- [13] Alexey Dosovitskiy, Lucas Beyer, Alexander Kolesnikov, Dirk Weissenborn, Xiaohua Zhai, Thomas Unterthiner, Mostafa Dehghani, Matthias Minderer, Georg Heigold, Sylvain Gelly, et al. An image is worth 16x16 words: Transformers for image recognition at scale. *arXiv preprint arXiv:2010.11929*, 2020. 5
- [14] Alexey Dosovitskiy, Lucas Beyer, Alexander Kolesnikov, Dirk Weissenborn, Xiaohua Zhai, Thomas Unterthiner, Mostafa Dehghani, Matthias Minderer, Georg Heigold, Sylvain Gelly, Jakob Uszkoreit, and Neil Houlsby. An image is worth 16x16 words: Transformers for image recognition at scale, 2021. 2
- [15] Patrick Esser, Robin Rombach, and Bjorn Ommer. Taming transformers for high-resolution image synthesis. In *Proceedings of the IEEE/CVF conference on computer vision and pattern recognition*, pages 12873–12883, 2021. 1, 2, 3, 5, 6, 9, 11
- [16] Lijie Fan, Tianhong Li, Siyang Qin, Yuanzhen Li, Chen Sun, Michael Rubinstein, Deqing Sun, Kaiming He, and Yonglong Tian. Fluid: Scaling autoregressive text-to-image generative models with continuous tokens. *arXiv preprint arXiv:2410.13863*, 2024. 3
- [17] Jian Han, Jinlai Liu, Yi Jiang, Bin Yan, Yuqi Zhang, Zehuan Yuan, Bingyue Peng, and Xiaobing Liu. Infinity: Scaling bit-wise autoregressive modeling for high-resolution image synthesis. *arXiv preprint arXiv:2412.04431*, 2024. 1, 3
- [18] Kaiming He, Xinlei Chen, Saining Xie, Yanghao Li, Piotr Dollár, and Ross Girshick. Masked autoencoders are scalable vision learners. In *Proceedings of the IEEE/CVF conference on computer vision and pattern recognition*, pages 16000–16009, 2022. 2
- [19] Wanggui He, Siming Fu, Mushui Liu, Xierui Wang, Wenyi Xiao, Fangxun Shu, Yi Wang, Lei Zhang, Zhelun Yu, Haoyuan Li, et al. Mars: Mixture of auto-regressive models for fine-grained text-to-image synthesis. *arXiv preprint arXiv:2407.07614*, 2024. 3
- [20] Martin Heusel, Hubert Ramsauer, Thomas Unterthiner, Bernhard Nessler, and Sepp Hochreiter. Gans trained by a two time-scale update rule converge to a local nash equilibrium. *Advances in Neural Information Processing Systems*, 30, 2017. 2, 6
- [21] Geoffrey E Hinton and Ruslan R Salakhutdinov. Reducing the dimensionality of data with neural networks. *science*, 313(5786):504–507, 2006. 2
- [22] Jonathan Ho and Tim Salimans. Classifier-free diffusion guidance. *arXiv preprint arXiv:2207.12598*, 2022. 6
- [23] Mengqi Huang, Zhendong Mao, Zhuowei Chen, and Yongdong Zhang. Towards accurate image coding: Improved autoregressive image generation with dynamic vector quantization. In *Proceedings of the IEEE/CVF Conference on Computer Vision and Pattern Recognition*, pages 22596–22605, 2023. 1, 2
- [24] Tero Karras, Samuli Laine, and Timo Aila. A style-based generator architecture for generative adversarial networks. In *Proceedings of the IEEE/CVF conference on computer vision and pattern recognition*, pages 4401–4410, 2019. 9
- [25] Dongwon Kim, Ju He, Qihang Yu, Chenglin Yang, Xiaohui Shen, Suha Kwak, and Liang-Chieh Chen. Democratizing text-to-image masked generative models with compact text-aware one-dimensional tokens. *arXiv preprint arXiv:2501.07730*, 2025. 2

- [26] Alex M Lamb, Anirudh Goyal ALIAS PARTH GOYAL, Ying Zhang, Saizheng Zhang, Aaron C Courville, and Yoshua Bengio. Professor forcing: A new algorithm for training recurrent networks. *Advances in neural information processing systems*, 29, 2016. 3
- [27] Christian Ledig, Lucas Theis, Ferenc Huszár, Jose Caballero, Andrew Cunningham, Alejandro Acosta, Andrew Aitken, Alykhan Tejani, Johannes Totz, Zehan Wang, et al. Photo-realistic single image super-resolution using a generative adversarial network. In *Proceedings of the IEEE conference on computer vision and pattern recognition*, pages 4681–4690, 2017. 9
- [28] Doyup Lee, Chiheon Kim, Saehoon Kim, Minsu Cho, and Wook-Shin Han. Autoregressive image generation using residual quantization. In *Proceedings of the IEEE/CVF Conference on Computer Vision and Pattern Recognition*, pages 11523–11532, 2022. 1, 2
- [29] Doyup Lee, Chiheon Kim, Saehoon Kim, Minsu Cho, and Wook-Shin Han. Autoregressive image generation using residual quantization, 2022. 6
- [30] Haopeng Li, Jinyue Yang, Kexin Wang, Xuerui Qiu, Yuhong Chou, Xin Li, and Guoqi Li. Scalable autoregressive image generation with mamba. *arXiv preprint arXiv:2408.12245*, 2024. 3
- [31] Tianhong Li, Dina Katabi, and Kaiming He. Return of unconditional generation: A self-supervised representation generation method, 2024. 6
- [32] Tianhong Li, Yonglong Tian, He Li, Mingyang Deng, and Kaiming He. Autoregressive image generation without vector quantization, 2024. 3, 6
- [33] Xiang Li, Jinglu Wang, Xiaohao Xu, Xiao Li, Bhiksha Raj, and Yan Lu. Robust referring video object segmentation with cyclic structural consensus. In *Proceedings of the IEEE/CVF International Conference on Computer Vision*, pages 22236–22245, 2023. 2
- [34] Xiang Li, Jinglu Wang, Xiaohao Xu, Muqiao Yang, Fan Yang, Yizhou Zhao, Rita Singh, and Bhiksha Raj. Towards noise-tolerant speech-referring video object segmentation: Bridging speech and text. In *Proceedings of the 2023 Conference on Empirical Methods in Natural Language Processing*, pages 2283–2296, 2023. 2
- [35] Xiang Li, Kai Qiu, Hao Chen, Jason Kuen, Jiuxiang Gu, Bhiksha Raj, and Zhe Lin. Imagefolder: Autoregressive image generation with folded tokens. *arXiv preprint arXiv:2410.01756*, 2024. 2, 5, 6, 9
- [36] Xiang Li, Kai Qiu, Hao Chen, Jason Kuen, Jiuxiang Gu, Jindong Wang, Zhe Lin, and Bhiksha Raj. Xq-gan: An open-source image tokenization framework for autoregressive generation. *arXiv preprint arXiv:2412.01762*, 2024. 2, 5, 6, 7, 9, 11
- [37] Xiang Li, Kai Qiu, Hao Chen, Jason Kuen, Zhe Lin, Rita Singh, and Bhiksha Raj. Controlvar: Exploring controllable visual autoregressive modeling. *arXiv preprint arXiv:2406.09750*, 2024. 3
- [38] Xiang Li, Kai Qiu, Jinglu Wang, Xiaohao Xu, Rita Singh, Kashu Yamazaki, Hao Chen, Xiaonan Huang, and Bhiksha Raj. R 2-bench: Benchmarking the robustness of referring perception models under perturbations. In *European Conference on Computer Vision*, pages 211–230. Springer, 2024. 2
- [39] Xiang Li, Jinglu Wang, Xiaohao Xu, Xiulian Peng, Rita Singh, Yan Lu, and Bhiksha Raj. Qdformer: towards robust audiovisual segmentation in complex environments with quantization-based semantic decomposition. In *Proceedings of the IEEE/CVF Conference on Computer Vision and Pattern Recognition*, pages 3402–3413, 2024. 2
- [40] Zhuoyan Luo, Fengyuan Shi, Yixiao Ge, Yujiu Yang, Limin Wang, and Ying Shan. Open-magvit2: An open-source project toward democratizing auto-regressive visual generation. *arXiv preprint arXiv:2409.04410*, 2024. 1, 2
- [41] Fabian Mentzer, David Minnen, Eirikur Agustsson, and Michael Tschannen. Finite scalar quantization: Vq-vae made simple, 2023. 3
- [42] Keita Miwa, Kento Sasaki, Hidehisa Arai, Tsubasa Takahashi, and Yu Yamaguchi. One-d-piece: Image tokenizer meets quality-controllable compression. *arXiv e-prints*, pages arXiv–2501, 2025. 1, 2
- [43] David Mizrahi, Roman Bachmann, Oguzhan Kar, Teresa Yeo, Mingfei Gao, Afshin Dehghan, and Amir Zamir. 4m: Massively multimodal masked modeling. *Advances in Neural Information Processing Systems*, 36, 2024. 3
- [44] Alex Nichol and Prafulla Dhariwal. Improved denoising diffusion probabilistic models, 2021. 1
- [45] J Ning, C Li, Z Zhang, Z Geng, Q Dai, K He, and H Hu. All in tokens: Unifying output space of visual tasks via soft token. arxiv 2023. *arXiv preprint arXiv:2301.02229*. 2
- [46] Maxime Oquab, Timothée Darcet, Theo Moutakanni, Huy V. Vo, Marc Szafraniec, Vasil Khalidov, Pierre Fernandez, Daniel Haziza, Francisco Massa, Alaaeldin El-Nouby, Russell Howes, Po-Yao Huang, Hu Xu, Vasu Sharma, Shang-Wen Li, Wojciech Galuba, Mike Rabbat, Mido Assran, Nicolas Ballas, Gabriel Synnaeve, Ishan Misra, Herve Jegou, Julien Mairal, Patrick Labatut, Armand Joulin, and Piotr Bojanowski. Dinov2: Learning robust visual features without supervision, 2023. 2, 5, 9
- [47] Yatian Pang, Peng Jin, Shuo Yang, Bin Lin, Bin Zhu, Zhenyu Tang, Liuhan Chen, Francis EH Tay, Ser-Nam Lim, Harry Yang, et al. Next patch prediction for autoregressive visual generation. *arXiv preprint arXiv:2412.15321*, 2024. 3
- [48] Ziqi Pang, Tianyuan Zhang, Fujun Luan, Yunze Man, Hao Tan, Kai Zhang, William T Freeman, and Yu-Xiong Wang. Randar: Decoder-only autoregressive visual generation in random orders. *arXiv preprint arXiv:2412.01827*, 2024. 3
- [49] William Peebles and Saining Xie. Scalable diffusion models with transformers, 2023. 1, 6
- [50] Kai Qiu, Xiang Li, Hao Chen, Jie Sun, Jinglu Wang, Zhe Lin, Marios Savvides, and Bhiksha Raj. Efficient autoregressive audio modeling via next-scale prediction. *arXiv preprint arXiv:2408.09027*, 2024. 1, 3
- [51] Alec Radford, Jong Wook Kim, Chris Hallacy, Aditya Ramesh, Gabriel Goh, Sandhini Agarwal, Girish Sastry, Amanda Askell, Pamela Mishkin, Jack Clark, et al. Learning transferable visual models from natural language supervision. In *International conference on machine learning*, pages 8748–8763. PMLR, 2021. 2

- [52] Ali Razavi, Aaron Van den Oord, and Oriol Vinyals. Generating diverse high-fidelity images with vq-vae-2. *Advances in neural information processing systems*, 32, 2019. 2
- [53] Ali Razavi, Aaron van den Oord, and Oriol Vinyals. Generating diverse high-fidelity images with vq-vae-2, 2019. 2
- [54] Sucheng Ren, Qihang Yu, Ju He, Xiaohui Shen, Alan Yuille, and Liang-Chieh Chen. Flowar: Scale-wise autoregressive image generation meets flow matching. *arXiv preprint arXiv:2412.15205*, 2024. 3
- [55] Sucheng Ren, Qihang Yu, Ju He, Xiaohui Shen, Alan Yuille, and Liang-Chieh Chen. Beyond next-token: Next-x prediction for autoregressive visual generation. *arXiv preprint arXiv:2502.20388*, 2025. 1
- [56] Robin Rombach, Andreas Blattmann, Dominik Lorenz, Patrick Esser, and Björn Ommer. High-resolution image synthesis with latent diffusion models, 2022. 1, 6
- [57] Tim Salimans, Ian Goodfellow, Wojciech Zaremba, Vicki Cheung, Alec Radford, and Xi Chen. Improved techniques for training gans. *Advances in Neural Information Processing Systems*, 29, 2016. 6
- [58] Fengyuan Shi, Zhuoyan Luo, Yixiao Ge, Yujia Yang, Ying Shan, and Limin Wang. Taming scalable visual tokenizer for autoregressive image generation. *arXiv preprint arXiv:2412.02692*, 2024. 5, 11
- [59] Jie Shi, Chenfei Wu, Jian Liang, Xiang Liu, and Nan Duan. Divae: Photorealistic images synthesis with denoising diffusion decoder, 2022. 3
- [60] Jiaming Song, Chenlin Meng, and Stefano Ermon. Denoising diffusion implicit models, 2022. 1
- [61] Peize Sun, Yi Jiang, Shoufa Chen, Shilong Zhang, Bingyue Peng, Ping Luo, and Zehuan Yuan. Autoregressive model beats diffusion: Llama for scalable image generation. *arXiv preprint arXiv:2406.06525*, 2024. 2, 3, 5, 6, 11
- [62] Richard S Sutton. Learning to predict by the methods of temporal differences. *Machine learning*, 3:9–44, 1988. 1, 3
- [63] Yuhta Takida, Yukara Ikemiya, Takashi Shibuya, Kazuki Shimada, Woosung Choi, Chieh-Hsin Lai, Naoki Murata, Toshimitsu Uesaka, Kengo Uchida, Wei-Hsiang Liao, et al. Hq-vae: Hierarchical discrete representation learning with variational bayes. *arXiv preprint arXiv:2401.00365*, 2023. 1, 2
- [64] Keyu Tian, Yi Jiang, Zehuan Yuan, Bingyue Peng, and Liwei Wang. Visual autoregressive modeling: Scalable image generation via next-scale prediction, 2024. 1, 3, 6
- [65] Shengbang Tong, David Fan, Jiachen Zhu, Yunyang Xiong, Xinlei Chen, Koustuv Sinha, Michael Rabbat, Yann LeCun, Saining Xie, and Zhuang Liu. Metamorph: Multimodal understanding and generation via instruction tuning. *arXiv preprint arXiv:2412.14164*, 2024. 3
- [66] Michael Tschannen, Cian Eastwood, and Fabian Mentzer. Givit: Generative infinite-vocabulary transformers. In *European Conference on Computer Vision*, pages 292–309. Springer, 2024. 3
- [67] Arash Vahdat, Karsten Kreis, and Jan Kautz. Score-based generative modeling in latent space, 2021. 1
- [68] Aaron Van den Oord, Nal Kalchbrenner, Lasse Espeholt, Oriol Vinyals, Alex Graves, et al. Conditional image generation with pixelcnn decoders. *Advances in neural information processing systems*, 29, 2016. 1, 3
- [69] Aäron Van Den Oord, Nal Kalchbrenner, and Koray Kavukcuoglu. Pixel recurrent neural networks. In *International conference on machine learning*, pages 1747–1756. PMLR, 2016. 1, 3
- [70] Aaron Van Den Oord, Oriol Vinyals, et al. Neural discrete representation learning. *Advances in neural information processing systems*, 30, 2017. 2
- [71] Ashish Vaswani, Noam Shazeer, Niki Parmar, Jakob Uszkoreit, Llion Jones, Aidan N. Gomez, Lukasz Kaiser, and Illia Polosukhin. Attention is all you need, 2023. 2, 3
- [72] Pascal Vincent, Hugo Larochelle, Yoshua Bengio, and Pierre-Antoine Manzagol. Extracting and composing robust features with denoising autoencoders. In *Proceedings of the 25th international conference on Machine learning*, pages 1096–1103, 2008. 2
- [73] Huiyu Wang, Yukun Zhu, Hartwig Adam, Alan Yuille, and Liang-Chieh Chen. Max-deeplab: End-to-end panoptic segmentation with mask transformers, 2021. 2
- [74] Yuqing Wang, Shuhuai Ren, Zhijie Lin, Yujin Han, Haoyuan Guo, Zhenheng Yang, Difan Zou, Jiashi Feng, and Xihui Liu. Parallelized autoregressive visual generation. *arXiv preprint arXiv:2412.15119*, 2024. 3
- [75] Zhou Wang, Alan C Bovik, Hamid R Sheikh, and Eero P Simoncelli. Image quality assessment: from error visibility to structural similarity. *IEEE transactions on image processing*, 13(4):600–612, 2004. 2
- [76] Mark Weber, Lijun Yu, Qihang Yu, Xueqing Deng, Xiaohui Shen, Daniel Cremers, and Liang-Chieh Chen. Maskbit: Embedding-free image generation via bit tokens. *arXiv preprint arXiv:2409.16211*, 2024. 1, 2, 6, 9
- [77] Junfeng Wu, Yi Jiang, Chuofan Ma, Yuliang Liu, Hengshuang Zhao, Zehuan Yuan, Song Bai, and Xiang Bai. Liq-uid: Language models are scalable multi-modal generators. *arXiv preprint arXiv:2412.04332*, 2024. 3
- [78] Xiaohao Xu, Tianyi Zhang, Shibo Zhao, Xiang Li, Sibowang, Yongqi Chen, Ye Li, Bhiksha Raj, Matthew Johnson-Roberson, Sebastian Scherer, et al. Scalable benchmarking and robust learning for noise-free ego-motion and 3d reconstruction from noisy video. In *The Thirteenth International Conference on Learning Representations*. 2
- [79] Lihe Yang, Bingyi Kang, Zilong Huang, Xiaogang Xu, Jiashi Feng, and Hengshuang Zhao. Depth anything: Unleashing the power of large-scale unlabeled data. In *Proceedings of the IEEE/CVF Conference on Computer Vision and Pattern Recognition*, pages 10371–10381, 2024. 2
- [80] Jingfeng Yao and Xinggang Wang. Reconstruction vs. generation: Taming optimization dilemma in latent diffusion models. *arXiv preprint arXiv:2501.01423*, 2025. 2
- [81] Lijun Yu, Yong Cheng, Kihyuk Sohn, José Lezama, Han Zhang, Huiwen Chang, Alexander G Hauptmann, Ming-Hsuan Yang, Yuan Hao, Irfan Essa, et al. Magvit: Masked generative video transformer. In *Proceedings of the IEEE/CVF Conference on Computer Vision and Pattern Recognition*, pages 10459–10469, 2023. 1, 2
- [82] Lijun Yu, José Lezama, Nitesh B. Gundavarapu, Luca Versari, Kihyuk Sohn, David Minnen, Yong Cheng, Agrim

- Gupta, Xiuye Gu, Alexander G. Hauptmann, Boqing Gong, Ming-Hsuan Yang, Irfan Essa, David A. Ross, and Lu Jiang. Language model beats diffusion – tokenizer is key to visual generation, 2023. [3](#), [6](#)
- [83] Lijun Yu, Yong Cheng, Zhiruo Wang, Vivek Kumar, Wolfgang Macherey, Yanping Huang, David Ross, Irfan Essa, Yonatan Bisk, Ming-Hsuan Yang, et al. Spae: Semantic pyramid autoencoder for multimodal generation with frozen llms. *Advances in Neural Information Processing Systems*, 36, 2024. [1](#), [2](#)
- [84] Qihang Yu, Ju He, Xueqing Deng, Xiaohui Shen, and Liang-Chieh Chen. Randomized autoregressive visual generation. *arXiv preprint arXiv:2411.00776*, 2024. [1](#), [2](#), [3](#), [6](#), [9](#)
- [85] Qihang Yu, Mark Weber, Xueqing Deng, Xiaohui Shen, Daniel Cremers, and Liang-Chieh Chen. An image is worth 32 tokens for reconstruction and generation, 2024. [5](#), [6](#), [11](#)
- [86] Kaiwen Zha, Lijun Yu, Alireza Fathi, David A Ross, Cordelia Schmid, Dina Katabi, and Xiuye Gu. Language-guided image tokenization for generation. *arXiv preprint arXiv:2412.05796*, 2024. [2](#)
- [87] Yue Zhao, Yuanjun Xiong, and Philipp Krähenbühl. Image and video tokenization with binary spherical quantization. *arXiv preprint arXiv:2406.07548*, 2024. [3](#)
- [88] Chuanxia Zheng, Long Tung Vuong, Jianfei Cai, and Dinh Phung. Movq: Modulating quantized vectors for high-fidelity image generation, 2022. [1](#), [2](#)
- [89] Lei Zhu, Fangyun Wei, Yanye Lu, and Dong Chen. Scaling the codebook size of vqgan to 100,000 with a utilization rate of 99%. *arXiv preprint arXiv:2406.11837*, 2024. [1](#), [2](#), [5](#), [11](#)
- [90] X Zhu, W Su, L Lu, B Li, X Wang, and J Dai. Deformable detr: Deformable transformers for end-to-end object detection. *arxiv* 2020. *arXiv preprint arXiv:2010.04159*, 2010. [2](#)
- [91] Yongxin Zhu, Bocheng Li, Yifei Xin, and Linli Xu. Addressing representation collapse in vector quantized models with one linear layer. *arXiv preprint arXiv:2411.02038*, 2024. [1](#), [2](#)
- [92] Yongxin Zhu, Bocheng Li, Hang Zhang, Xin Li, Linli Xu, and Lidong Bing. Stabilize the latent space for image autoregressive modeling: A unified perspective. *arXiv preprint arXiv:2410.12490*, 2024. [2](#)